An explanation of episodic tremor and slow slip constrained by crack-seal veins and viscous shear in subduction mélange

Kohtaro Ujiie[1,2*], Hanae Saishu[3,4], Åke Fagereng[5], Naoki Nishiyama[1], Makoto Otsubo[4], Haruna Masuyama[1], and Hiroyuki Kagi[6]

[1] Graduate School of Life and Environmental Sciences, University of Tsukuba, Japan.
[2] Research and Development Center for Ocean Drilling Science, Japan Agency for Marine-Earth Science and Technology, Japan.
[3] Renewable Energy Research Center, National Institute of Advanced Industrial Science and Technology, Japan.
[4] Geological Survey of Japan, National Institute of Advanced Industrial Science and Technology, Japan.
[5] School of Earth and Ocean Sciences, Cardiff University, UK.
[6] Geochemical Research Center, Graduate School of Science, The University of Tokyo, Japan.

*Corresponding author: Kohtaro Ujiie (kujiie@geol.tsukuba.ac.jp)

Key Points:

- Crack-seal veins in subduction mélange record repeated low-angle thrust faulting under tensile overpressure
- The minimum time interval between thrusting events is comparable to recurrence intervals of slow earthquakes
- Crack-seal veins and viscous shear zones in subduction mélange may be geological manifestations of episodic tremor and slow slip

Abstract

Episodic tremor and slow slip (ETS) occurs in the transition zone between the locked seismogenic zone and the deeper, stably sliding zone. Actual mechanisms of ETS are enigmatic, caused by lack of geological observations and limited spatial resolution of geophysical information from the ETS source. We report that quartz-filled, crack-seal shear and extension veins in subduction mélange record repeated low-angle thrust-sense frictional sliding and tensile fracturing at near-lithostatic fluid pressures. Crack-seal veins were coeval with viscous shear zones that accommodated deformation by pressure solution creep. The minimum time interval between thrusting events, determined from a kinetic model of quartz precipitation in shear veins, was less than a few years. This short recurrence time of low-angle brittle thrusting at near-lithostatic fluid overpressures within viscous shear zones may be explained by frequent release of accumulated strain by ETS.

1. Introduction

A spectrum of slow earthquake behaviors, including low-frequency tectonic tremors (LFTs), low-frequency earthquakes (LFEs), very-low-frequency earthquakes (VLFEs), and slow slip events (SSEs), has been detected from seismologic and geodetic observations [*Schwartz and Rokosky*, 2007; *Peng and Gomberg*, 2010; *Beroza and Ide*, 2011; *Saffer and Wallace*, 2015; *Obara and Kato*, 2016]. Tectonic tremor is defined as a persistent low frequency seismic signal that lasts for days to weeks but is interpreted to

represent a swarm of LFEs that accommodate shear slip on low-angle thrusts [*Shelly et al*., 2007; *Ide et al*., 2007]. Slow slip is a geodetically detected, transient creep event where slip speed exceeds average plate motion but is too slow to generate detectable seismic waves. On some faults, slow slip events appear to repeat near-periodically in the same location, and in some places these events are spatiotemporally accompanied by LFTs, referred to as episodic tremor and slow slip (ETS) [*Rogers and Dragert*, 2003; *Obara et al*., 2004].

In subduction zones, slow earthquake phenomena generally occur in transition zones between interseismically locked and stably sliding fault segments [*Schwartz and Rokosky*, 2007; *Peng and Gomberg*, 2010]. ETS events are typically observed along the plate boundary thrust near the mantle wedge corner in relatively warm subduction zones. These events repeat at least every few years, and thus lead to episodic transfer of stress from the ETS region to the locked seismogenic zone; this stress change may contribute to trigger megathrust earthquakes [*Obara and Kato*, 2016]. Recent studies in the Nankai subduction zone have revealed that LFTs, LFEs, and SSEs occur along the plate boundary at depths of ~6–9 km and ~15 km [*Yamashita et al*., 2015; *Araki et al*., 2017; *Nakano et al*., 2018]. The components of ETS can therefore be generated along the plate boundary at depths much shallower than the mantle wedge corner.

Despite the importance for understanding the dynamics of slow earthquakes and their relation to megathrust earthquakes, the underlying deformation mechanisms responsible for slow earthquake-generated deformation remain poorly understood. This shortfall in physical understanding arises from insufficient geological information on

slow earthquakes, limited constraint on the temporal relationship between slow earthquakes and ordinary megathrust earthquakes, and poor spatial constraints on the source area of slow earthquakes and the spatiotemporal relation between tremor and slow slip. Whereas geological evidence for high-speed slip, such as pseudotachylyte (solidified frictional melt produced by seismic slip), has been reported from subduction zones [*Ujiie et al*., 2007; *Ujiie and Kimura*, 2014], low-speed deformation responsible for slow earthquakes have been attributed to brittle failure of relatively strong lenses coincident with viscous shear in surrounding matrix [*Skarbek et al*., 2012; *Fagereng et al*., 2014; *Hayman and Lavier*, 2014; *Behr et al*., 2018].

The exhumed Makimine mélange in the Late Cretaceous Shimanto accretionary complex of eastern Kyushu, southwest Japan (Figure 1) records progressive plate boundary deformation during subduction of young, warm oceanic crust to a shallow (10–15 km) frictional-viscous transition where temperatures reached 300–350 °C [*Mackenzie et al*., 1987; *Hara and Kimura*, 2008; *Palazzin et al*., 2016]. This mélange is exhumed from a frictional-viscous transition zone, typical of where slow earthquakes commonly occur. We examine the potential record of slow earthquakes by considering four key geophysical observations from active subduction margins [*Rogers and Dragert*, 2003; *Obara et al*., 2004; *Schwartz and Rokosky*, 2007; *Peng and Gomberg*, 2010; *Beroza and Ide*, 2011; *Saffer and Wallace*, 2015; *Obara and Kato*, 2016; *Wallace et al*., 2016; *Araki et al*., 2017]: (1) slow earthquakes typically occur in regions of high fluid pressure and low effective stress; (2) VLFEs, and triggered swarms of LFEs associated with SSEs, have very low stress drops (tens of kilopascal) implying that the effective

92 fault strength is very weak and sensitive to perturbations; (3) when the focal mechanism
93 is determined, slow earthquakes commonly exhibit shear slip on low-angle thrust faults
94 subparallel to the plate boundary interface; and (4) ETS events repeat every several
95 months to a few years.
96
97 **2. Geological setting**
98 The Shimanto accretionary complex distributed along the Pacific side of southwest
99 Japan has been believed to represent an ancient on-land analog of the Nankai Trough
100 subduction zone (Figure 1a) [*Ujiie and Kimura*, 2014]. The Makimine mélange in the
101 Shimanto accretionary complex of eastern Kyushu is Cenomanian to
102 Campanian/Maastrichian in age (Late Cretaceous) and experienced prehnite-actinolite
103 to greenschist facies metamorphism at 10–15 km depth [*Hara and Kimura*, 2008;
104 *Palazzin et al*., 2016]. The maximum temperatures determined from Raman spectra of
105 carbonaceous material, vitrinite reflectance, and illite crystallinity range from 300 to
106 350 °C [*Hara and Kimura*, 2008; *Palazzin et al*., 2016; supporting information]. The
107 mélange generally dips north-northwestward. The Makimine mélange preserves ocean
108 plate stratigraphy composed, in ascending order, of (1) mudstone-dominated mélange
109 containing basalt lenses and hemipelagic red mudstone at the base, (2) reddish brown
110 tuff, and (3) sandstone-mudstone mélange and coherent turbidites (Figure 1b). This
111 stratigraphy is repeated at least twice along the coastal exposure, possibly caused by
112 duplex underplating after subduction, with the apparent thickness of each thrust sheet in
113 the range 1300–1600 m. The subduction-related deformation at the frictional-viscous

114 transition is well preserved [*Mackenzie et al*., 1987; *Palazzin et al*., 2016]. Stretching
115 lineations defined by aligned mica prisms, quartz rods, and long axes of sandstone
116 blocks are particularly well developed in the structurally lower part of the mélange
117 (Figure 1c). This lineation represents constrictional strain and is interpreted as parallel
118 to the tectonic transport direction during subduction-related deformation, and indicates
119 that the subduction direction was perpendicular to the general strike of the mélange
120 (Figure 1d).
121

122 **3. Crack-seal veins and viscous shear zones in subduction mélange**

123 A 10–60 m thick zone where quartz veins are highly concentrated occurs in the
124 lower part of the Makimine mélange, within which a penetrative foliation is defined by
125 pressure solution cleavage (Figure 1b). Along-strike continuity and across-strike
126 structural repetition of the vein concentration zone, and no spatial correlation between
127 the vein distribution zone and the thrust accommodating underplating, indicate that the
128 zone of vein concentration was formed during subduction and prior to the underplating
129 that incorporated the mélange into the overlying accretionary prism (Figure 1b). Shear
130 veins, foliation-parallel extension veins, subvertical extension veins, and viscous shear
131 zones are recognized within the vein concentration zone (Figure 2).

132 Shear veins are subparallel to the mélange foliation, with along-strike length ranging
133 from 1 to 10 m (typically about 1 m) (Figures 2a and 3a). Shear veins are laminated and
134 fibrous (Figure 2b), representing multiple episodes of dilation and quartz precipitation
135 along shear surfaces. The internal texture of shear veins is characterized by crack-seal

texture defined by phyllosilicate inclusion bands subparallel to vein margins, with spacing ranging from 20 to 38 μm (Figure 2c and supporting information). At dilational stepovers, the inclusion bands are oblique to vein margins, and slip increments determined from fiber growth increments are 0.1–0.2 mm (Figure 2d). On the basis of the dip direction of inclusion bands at dilational stepovers and steps on the vein surfaces, shear veins exhibit thrust shear sense (Figures 2b and 2d). Slickenfiber orientations are consistent with the top-SSE shear direction determined from the trend of stretching lineations (Figures 1d and 3a). Tectonic reconstructions indicate subduction towards the NNW [*Whittaker et al*., 2007; *Müller et al*., 2008], consistent with top-SSE shear, and thus the kinematics of both stretching lineations and localized, frictional shear veins are compatible with low-angle thrust faulting during subduction.

Foliation-parallel extension veins also show crack-seal texture marked by development of inclusion bands of ~28–42 μm spacing but lack dilational stepovers and slickenfibers on vein surfaces (Figure 2a). The length of foliation-parallel extension veins along strike is typically ~1 m, similar to that of shear veins. Subvertical extension veins are straight or sigmoidal, commonly constituting localized *en echelon* arrays (Figure 2e). Quartz crystals within the subvertical veins are elongate with long axes perpendicular to vein margins (Figure 2f), and a crack-seal texture is defined by 25 μm spaced inclusion bands aligned parallel to vein boundaries. Viscous shear zones are defined by < 10 m thick zones of rotated mélange foliations (Figure 2g). The viscous deformation is accommodated by pressure solution creep, illustrated by dark selvages and precipitates in pressure shadows, and commonly shows thrust shear sense. Some

158 shear veins, subhorizontal extension veins, and subvertical extension veins cut the
159 asymmetric fabric formed by viscous shear (Figure 2h), but are also themselves
160 viscously deformed (Figure 2g). These features indicate that brittle shear slip with
161 tensile fracturing and viscous shear occurred contemporaneously.
162
163 **4. Low-angle thrust faulting under tensile overpressure**
164 Pressure solution cleavage forms perpendicular to the greatest principal
165 compressive stress (σ_1) and thus the low-angle foliation implies a subvertical σ_1,
166 consistent with subvertical extension veins. However, this foliation reflects finite strain
167 and may therefore reflect long-term subvertical shortening, rather than stresses driving
168 fracturing [e.g. *Fisher and Byrne*, 1987; *Ujiie*, 2002; *Fagereng*, 2013]. It is conceivable
169 that σ_1 was consistently subvertical and foliation-parallel extension veins involved
170 opening of low cohesion, weak planes. However, this interpretation becomes
171 problematic, because (1) it requires σ_1 to become tensile, and (2) it is difficult to explain
172 the gentle dip of crack-seal bands within shear veins and foliation-parallel extension
173 veins. We therefore suggest that the stress repeatedly rotated, which resulted in
174 subvertical extension veins and foliation-parallel extension veins formed in different
175 stress fields. As pointed out by *Meneghini and Moore* [2007], both explanations above
176 require cyclicity in effective normal stress.
177 A very small angle (~5.5°) between the average orientations of shear veins and
178 foliation-parallel extension veins indicates that shear veins were formed as hybrid
179 extensional-shear fractures under low differential stress of $4T_0 < \Delta\sigma < 5.66T_0$ [*Secor*,

180 1965], where T_0 is the rock tensile strength, and $\Delta\sigma$ is the differential stress (Figures 3a–
181 3c). This is consistent with that shear veins opened at a high angle to the vein margin
182 (Figure 2c). The geometrical relation between shear veins and foliation-parallel
183 extension veins may represent fault-fracture meshes developed in a compressional
184 regime [*Sibson*, 2017], where thrust faults lie at very low angles to σ_1, and the least
185 principal compressive stress (σ_3) is approximately equal to the vertical stress (σ_V)
186 (Figure 3d). Under such a compressional regime, shear veins and hydraulic extension
187 veins are expected to develop at near-lithostatic and supralithostatic fluid overpressures,
188 respectively, as a result of opening directions of subhorizontal tensile veins being
189 subparallel to the subvertical σ_3. Supposing T_0 = 1 MPa, a low estimate for typical
190 pelitic rocks [*Lockner*, 1995] to account for the deformed nature of mélange mudstones,
191 shear strength (τ) at a very low angle to σ_1 (5.5°) is extremely low, $0.38 < \tau < 0.54$ MPa.
192 In this model, the mutually crosscutting relationship between the shear veins and local
193 arrays of subvertical tensile veins, as well as the presence of stylolites and folded
194 phyllosilicate inclusion bands in shear veins (Figure 2d), imply that the local stress field
195 could transiently swap between vertical σ_3 and vertical σ_1, which is also indicative of
196 low differential stress. If, like *Fagereng et al*. [2011], we assume a low shear modulus
197 of 3 GPa for the mélange rocks, the stress drop for 0.1–0.2 mm slip increments on 1–10
198 m long faults is 30–600 kPa, consistent with very low driving stresses.

199 The observations and model presented here differ in geometry from that
200 described by *Fagereng et al*. [2011]. The vein system they describe, in the Chrystalls
201 Beach Complex, New Zealand, consistently shows coeval shear and extension veins

formed under a subvertical σ_1. The steep σ_1 determined in the Chrystalls Beach Complex is typical of weak, underthrust sediments [e.g. *Fisher and Byrne*, 1987], consistent also with thrust faults there developed along weak, low cohesion, clay-rich cleavage [*Fagereng et al*., 2010]. In the Makimine mélange, a horizontal σ_1 explains many of the brittle structures, but episodically the stress field switched to vertical σ_1. This may be a dynamic effect, as also seen in focal mechanisms before and after the 2011 Tohoku-Oki earthquake [e.g., *Hasegawa et al*., 2011; *Lin et al*., 2013]. Why the dominant stress field differs between Chrystalls Beach mélange and Makimine mélange shear veins is unclear, but may relate to differences in the frictional strength of the fault surfaces or the bulk rheology of the mélanges. In both cases, however, thrust sense faulting occurred episodically at low differential stress and near-lithostatic fluid pressure.

5. Time interval between crack-seal events

The crack-seal textures in shear and extension veins indicate that discontinuous deformation occurred repeatedly and we interpret the repetition to correlate with temporal fluid pressure variations. To investigate the time required between each crack-seal event, a kinetic model for quartz precipitation [*Rimstidt and Barnes*, 1980], driven by movement of fluid down a pressure gradient, was applied for quartz-filled shear veins (supporting information). The model considers the width of inclusion bands in shear veins (20–38 μm), the typical length of shear veins (1 m), fluid pressure reduction at the start of each crack-seal event, and ambient temperature of 300–330 °C

224 (supporting information). Assuming that subhorizontal tensile fractures require at least
225 lithostatic fluid pressures, and that opening of these fractures creates at least temporarily
226 an interconnected fluid pathway, we consider a local fluid pressure change equal to
227 lithostatic minus hydrostatic pressure at the time of fracture opening. At 10–15 km
228 depth with average rock density of 2600 kg/m^3, this is a fluid pressure drop of 157–235
229 MPa. This large fluid pressure drop is consistent with various vapor/liquid ratios in
230 two-phase fluid inclusions within shear veins (supporting information). Assuming
231 precipitation rate controls the time of healing (i.e. silica can be transported to the open
232 fracture at least as far as quartz precipitates), the veins can close in less than 1.6–4.5
233 years (Figure 4). Quartz crystals are blocky and do not show collapse structures, which
234 is consistent with precipitation in an open crack that did not collapse. This lack of
235 collapse structures may be surprising upon a large fluid pressure drop, but could
236 possibly be explained by relatively fast precipitation from fluids moving through the
237 fracture system in response to increased fracture permeability [cf. *Vrolijk*, 1987]. On the
238 other hand, we note that the large fluid pressure drop may have limited crack
239 propagation and locally arrested shear displacement. We thus assume this ≤ 1.6–4.5
240 years estimate corresponds to minimum healing time between deformation events. If the
241 fluid temperature is higher than ambient temperature, the model suggests that healing
242 time becomes shorter, and similarly, if precipitation is coupled to collapse of pore space
243 under increasing effective normal stress, healing rates will also increase [*Rimstidt and*
244 *Barnes*, 1980].
245

6. Discussion and Conclusion

Our results show that shear veins in subduction mélange record low-angle thrust faulting at very small shear strength and near-lithostatic fluid overpressures, consistent with plate boundary shear kinematics and key geophysical observations of slow earthquakes in subduction zones. The time required between discrete vein opening events, assuming complete healing of cracks defined by inclusion band spacing, gives a constraint of ≤ 1.6–4.5 years for the minimum time interval of repeated thrust faulting events. This repeat time is comparable to recurrence intervals of slow earthquakes. A large number (~100–150) of inclusion bands in shear veins (supporting information) indicate multiple occurrences of fracturing under elevated fluid pressure and subsequent restoration of cohesive and tensile strength through hydrothermal precipitation. If the slip increment of ~0.1–0.2 mm at dilational stepovers correspond to the shear displacement during a single slow earthquake, ~100–150 inclusion bands suggest that cumulative displacement along individual low-angle thrust faults is ~0.01–0.03 m. Alternatively, the total displacement during a single slow earthquake event may be distributed into many different shear surfaces. In this case, the slip increment of ~0.1–0.2 mm during one crack-seal event could accommodate a small component of the total displacement during that slow earthquake. Crack-seal shear and extension veins are also recognized in other mélanges and metamorphic rocks exhumed from the source depths of slow earthquakes [*Fagereng et al*., 2011; *Fisher and Brantley*, 2014; *Sibson*, 2017]. Such crack-seal veins may also record repeated slow earthquake events.

In the Makimine mélange, the intensely veined zone is tens of meters thick, and involves a combination of viscous and frictional deformation. Such frictional-viscous deformation zones that are narrower than the full width of a mélange shear zone have been reported from other exhumed subduction zones, irrespective of deformation mechanisms of pressure solution creep or dislocation creep [*Rowe et al*., 2013; *Fagereng et al*., 2014]. Within a mélange shear zone, frictional-viscous deformation along narrow zones could represent deformation at higher strain rates. The absence of geological evidence of frictional heat (e.g. pseudotachylytes) in narrow shear zones suggests that strain rate is slower than seismic slip rate. Therefore, if localization of viscous shear into narrow zones implies higher strain rates [cf. *Fagereng et al*., 2014], then these may be candidates for slow earthquake zones. A common feature is coexistence of mineralized veins and relatively intense viscous fabrics, implying locally elevated fluid pressures and increased viscous strains, respectively. The geophysically observed signature of such deformation may be transient slow slip faster than plate motion rates (SSEs) accompanied by localized frictional failure (tremor containing LFEs).

Acknowledgements. This work is supported by Japan Society for the Promotion of Science KAKENHI grant JP16H06476. A.F. is supported by ERC Starting Grant 715836 “MICA”. Structural, Raman, and fluid inclusion data, and parameters and values used in the kinetic modeling are available in the supplementary materials. J. Kirkpatrick and an anonymous reviewer provided valuable comments that significantly improved the manuscript. We thank GRL Editor Lucy Flesch for evaluation of the paper.

We would also like to thank K. Ohta, Y. Yamashita, S. Katakami, and Y. Ito for valuable discussions.

References

Akinfiev, N. N., and L. W. Diamond (2009), A simple predictive model of quartz solubility in water-salt-CO2 systems at temperatures up to 1000 °C and pressures up to 1000 MPa, *Geochim. Cosmochim. Acta, 73*, 1597–1608.

Araki, E., et al. (2017), Recurring and triggered slow-slip events near the trench at the Nankai Trough subduction megathrust, *Science, 356*, 1157–1160.

Behr, W. M., A. J. Kotowski, and K. T. Ashley (2018), Dehydration-induced rheological heterogeneity and the deep tremor source in warm subduction zones, *Geology, 46*, https://doi.org/10.1130/G40105.1.

Beroza, G. C., and S. Ide (2011), Slow earthquakes and nonvolcanic tremor, *Annu. Rev. Earth Planet. Sci*., *39*, 271–296.

Fagereng, A. (2013), On stress and strain in a continuous-discontinuous shear zone undergoing simple shear and volume loss, *J. Struct. Geol*., *50*, 44–53.

Fagereng, A., F. Remitti, R. H. Sibson (2010), Shear veins observed within anisotropic fabric at high angles to the maximum compressive stress, *Nat. Geosci.*, *3*, 482–485.

Fagereng, A., F. Remitti, R. H. Sibson (2011), Incrementally developed slickenfibres–Geological record of repeating low stress-drop seismic events, *Tectonophysics*, *510*, 381–386.

310 Fagereng, A., G. W. B. Hillary, J. F. A. Diener (2014), Brittle-viscous deformation, slow slip,
311 and tremor, *Geophys. Res. Lett.*, *41*, 4159–4167.
312 Fisher, D., and T. Byrne (1987), Structural evolution of underthrusted sediments, Kodial
313 Island, Alaska, *Tectonics*, *6*, 775–793.
314 Fisher, D. M., and S. L. Brantley (2014), The role of silica redistribution in the evolution of
315 slip instabilities along subduction interfaces: Constraints from the Kodiak accretionary
316 complex, Alaska, *J. Struct. Geol.*, *69*, 395–414.
317 Hara, H., and K. Kimura (2008), Metamorphic and cooling history of the Shimanto
318 accretionary complex, Kyushu, Southwest Japan: Implications for the timing of
319 out-of-sequence thrusting, *Isl. Arc, 17*, 546–559.
320 Hasegawa, A., K. Yoshida, and T. Okada (2011), Nearly complete stress drop in the 2011 M_w
321 9.0 off the Pacific coast of Tohoku earthquake, *Earth Planets Space, 69*, 703–707.
322 Hayman, N. W., and L. L. Lavier (2014), The geological record of deep episodic tremor and
323 slip, *Geology, 42*, 195–198.
324 Ide, S., D. R. Shelly, and G. C. Beroza (2007), Mechanism of deep low frequency
325 earthquakes: Further evidence that deep non-volcanic tremor is generated by shear slip
326 on the plate interface, *Geophys. Res. Lett.*, *34*, L03308.
327 Kagi, H. et al. (1994), Proper understanding of down-shifted Raman spectra of natural
328 graphite: Direct estimation of laser-induced rise in sample temperature, *Geochim.*
329 *Cosmochim. Acta, 58*, 3527–3530.
330 Kouketsu, Y. et al. (2014), A new approach to develop the Raman carbonaceous material
331 geothermometer for low-grade metamorphism using peak width, *Isl. Arc, 23*, 33–50.

332 Lahfid, A. et al. (2010), Evolution of the Raman spectrum of carbonaceous material in
333 low-grade metasediments of the Glarus Alps (Switzerland), *Terra Nova, 22*, 354–360.
334 Lin, W., et al. (2013), Stress state in the largest displacement area of the 2011 Tohoku-Oki
335 earthquake, *Science, 339*, 687–690.
336 Lockner, D. A. *Rock Physics and Phase Relations, A Handbook of Physical Constants*, 127–
337 147 (AGU, 1995).
338 Mackenzie, J. S., D. T. Needham, and S. M. Agar (1987), Progressive deformation in an
339 accretionary complex: An example from the Shimanto belt of eastern Kyushu,
340 southwest Japan, *Geology, 15*, 353–356.
341 Meneghini, F. and J. C. Moore (2007), Deformation and hydrofracture in a subduction thrust
342 at seismogenic depths: The Rodeo Cove thrust zone, Marin Headlands, California, *GSA*
343 *Bulletin, 119*, 174-183.
344 Müller, R. D., et al. (2008), Long-term sea-level fluctuations driven by ocean basin dynamics,
345 *Science, 319,* 1357–1362.
346 Nakano, M., T. Hori, E. Araki, S. Kodaira, and S. Ide (2018), Shallow very-low-frequency
347 earthquakes accompany slow slip events in the Nankai subduction zone, *Nat. Commun.,*
348 *984*, doi:10.1038/s41467-018-03431-5.
349 Obara, K., and A. Kato (2016), Connecting slow earthquakes to huge earthquakes, *Science,*
350 *353*, 253–257.
351 Obara, K., H. Hirose, F. Yamamizu, and K. Kasahara (2004), Episodic slow slip events
352 accompanied by non-volcanic tremors in southwest Japan subduction zone, *Geophys.*
353 *Res. Lett*., *31*, L23602.

354 Okamoto, A. and K. Sekine (2011), Textures of syntaxial quartz veins synthesized by
355 hydrothermal experiments, *J. Struct. Geol.*, *33*, 1764–1775.
356 Okamoto, A., H. Saishu, N. Hirano, and N. Tsuchiya (2010), Mineralogical and textural
357 variation of silica minerals in htdrothermal flow-through experiments: Implications for
358 quartz vein formationm *Geochim. Cosmochim. Acta, 74*, 3692–3706.
359 Palazzin, G., et al. (2016), Deformation processes at the down-dip limit of the seismogenic
360 zone: The example of Shimanto accretionary complex, *Tectonophysics, 687*, 28–43.
361 Peng, Z., and J. Gomberg (2010), An integrated perspective of the continuum between
362 earthquakes and slow slip phenomena, *Nat. Geosci*., *3,* 599–607.
363 Rimstidt, J. D., and H. L. Barnes (1980), The kinetics of silica-water reactions, *Geochim.*
364 *Cosmochim. Acta, 44*, 1683–1699.
365 Rogers, G., and H. Dragert (2003), Episodic tremor and slip on the Cascadia subduction zone:
366 The chatter of silent slip, *Science, 300*, 1942–1943.
367 Rowe, C. D., J. C. Moore, F. Remitti, and the IODP Expedition 343/343T Scientists (2013),
368 The thickness of subduction plate boundary faults from the seafloor into the
369 seismogenic zone, *Geolo*gy, *41*, 991–994.
370 Saffer, D. M., and L. M. Wallace (2015), The frictional, hydrological, metamorphic and
371 thermal habitat of shallow slow earthquakes, *Nat. Geosci*., *8*, 594–600.
372 Schwartz, S. Y., and J. M. Rokosky (2007), Slow slip events and seismic tremor at
373 circum-pacific subduction zones, *Rev. Geophys*., *45*, RG3004.
374 Secor, D. T. (1965), Role of fluid pressure in jointing, *Am. J. Sci*., *263*, 633–646.

375 Shelly, D. R., G. C. Beroza, and S. Ide (2007), Non-volcanic tremor and low-frequency
376 earthquakes swarms, *Nature, 446*, 305–307.
377 Sibson, R. H. (2017), Tensile overpressure compartments on low-angle thrust faults, *Earth*
378 *Planets Space, 69*, 113.
379 Skarbek, R. M., A. W. Rempel, and D. A. Schmidt (2012), Geologic heterogeneity can
380 produce aseismic slip transients, *Geophys. Res. Lett*., *39*, L21306.
381 Ujiie, K. (2002), Evolution and kinematics of an ancient décollement zone, mélange in the
382 Shimanto accretionary complex of Okinawa Island, Ryukyu Arc, *J. Struct. Geol*., *24*,
383 937–952.
384 Ujiie, K., and G. Kimura (2014), Earthquake faulting in subduction zones: Insights from fault
385 rocks in accretionary prisms, *Prog Earth Planet. Sci, 1*, 1–30,
386 doi:10.1186/2197-4284-1-7.
387 Ujiie, K., H. Yamaguchi, A. Sakaguchi, and S. Toh (2007), Pseudotachylytes in an ancient
388 accretionary complex and implications for melt lubrication during subduction zone
389 earthquakes, *J. Struct. Geol*., *29*, 599–613.
390 Vrolijk, P. (1987), Tectonically driven fluid flow in the Kodiak accretionary complex, Alaska,
391 *Geology*, *15*, 466-469.
392 Wallace, L. M., et al. (2016), Slow slip near the trench at the Hikurangi subduction zone, New
393 Zealand, *Science, 352*, 701–704.
394 Whittaker, J. M., et al. (2007), Major Australian-Antarctic plate reorganization at
395 Hawaiian-Emperor bend time, *Science, 318*, 83–86.

396 Yamashita, Y., et al. (2015), Migrating tremor off southern Kyushu as evidence for slow slip
397 of a shallow subduction interface, *Science, 348*, 676–679.
398

399 **Figure 1.** The Makimine mélange in the Shimanto accretionary complex. (a)
400 Distribution of the Shimanto accretionary complex in southwest Japan. (b) Geological
401 map of the Makimine mélange along the east coast of Kyushu. The location of the map
402 is shown in Fig. 1a. (c) Stretching lineations developed on the surface of mélange
403 foliation. The pencil is parallel to NNW-SSE oriented stretching lineations. The brighter
404 bands represent intersection between foliation and kink bands. (d) Lower hemisphere
405 equal-area stereoplots showing orientation of stretching lineations in the mélange.
406
407 **Figure 2.** Representative deformation in subduction mélange. Half arrows indicate
408 sense of shear. FPEV, Foliation-parallel extension veins. (a) Macroscopic appearance of
409 a shear vein and FPEV along the strike. (b) Slikenfibers and step (black arrow)
410 developed on the surface of shear vein, showing thrust sense of shear. (c) Microscopic
411 appearance of a shear vein cut parallel to slickenfibers and perpendicular to the shear
412 surface under cross-polarized light, showing repeated episodes of cracking and sealing.
413 The near-parallelism between phyllosilicate inclusion bands (black arrow) and the vein
414 margin indicates that the shear vein open at a high angle to the vein margin,
415 representing a hybrid extensional-shear fracture. (d) Folded phyllosilicate inclusion
416 bands (black arrow) at dilational stepovers under plane-polarized light. The horizontal
417 dark lines represent stylolites. (e) Macroscopic appearance of subvertical extension
418 veins along the dip showing *en echelon* arrays. (f) Microscopic appearance of a
419 subvertical extension vein under cross-polarized light. (g) Macroscopic appearance of a
420 viscous shear zone along the dip showing thrust sense of shear. (h) Microscopic

421 appearance of a viscous shear zone under plane-polarized light, showing the
422 development of asymmetric pressure solution fabric cut by subhorizontal extension
423 veins.
424
425 **Figure 3.** Low-angle thrust faulting at a very low angle to σ_1 under tensile overpressure.
426 (a) Lower hemisphere equal-area stereoplots showing orientation of slickenfiber shear
427 veins, mélange foliation, and average orientations of slickenfiber shear veins and
428 mélange foliation in the vein concentration zone in the lower thrust sheet. (b) Schematic
429 of geometrical relation between shear veins and foliation-parallel extension veins in a
430 compressional regime with $\sigma_3 = \sigma_V$. (c) Mohr diagram showing conditions of a hybrid
431 extensional-shear fracture at a very low angle to σ_1. τ, shear stress; σ_n', effective normal
432 stress. (d) Schematic of fault-fracture meshes developed along the subduction plate
433 boundary.
434
435 **Figure 4.** Sealing time for the width (*w*) of inclusion bands in quart-filled shear veins.
436 (a) At depth of 10 km and temperature of 300 °C. (b) At depth of 15 km and
437 temperature of 330 °C.

Figure 1.

a

134°E

34°N

Honshu

Shikoku

Kyushu

Fig. 1b

Nankai Trough

Tertiary Shimanto accretionary complex

Cretaceous Shimanto accretionary complex

Sandstone-mudstone mélange and bedded sandstone and mudstone

Reddish brown tuff

Mudstone-dominated mélange

Light grayish chert

Reddish mudstone

Basalt

Strike and dip of bedding

Strike and dip of foliation

Thrust fault

Vein concentration zone

b

c

d

Figure 2.

a

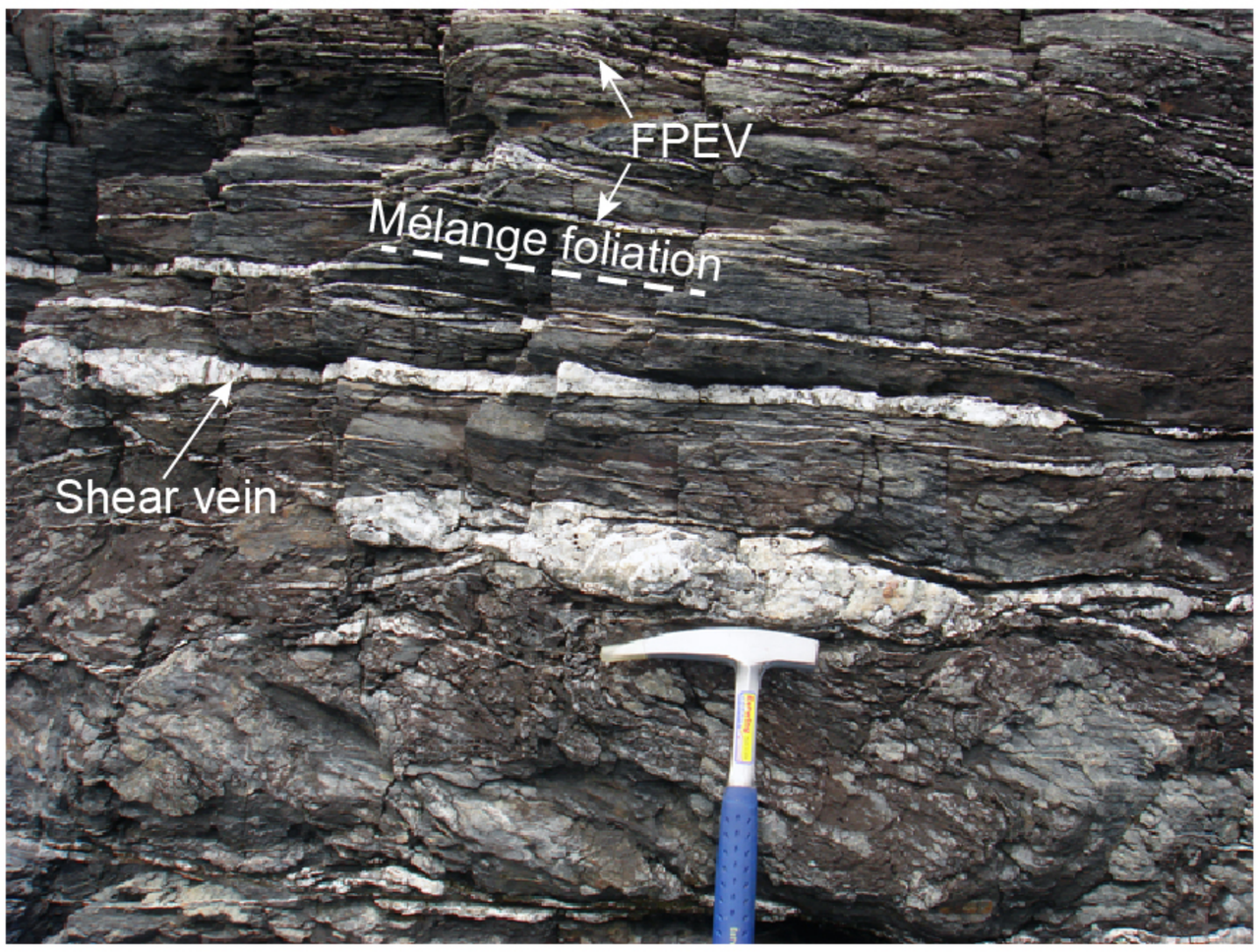
FPEV
Mélange foliation
Shear vein

b


STAINLESS
STEEL

c

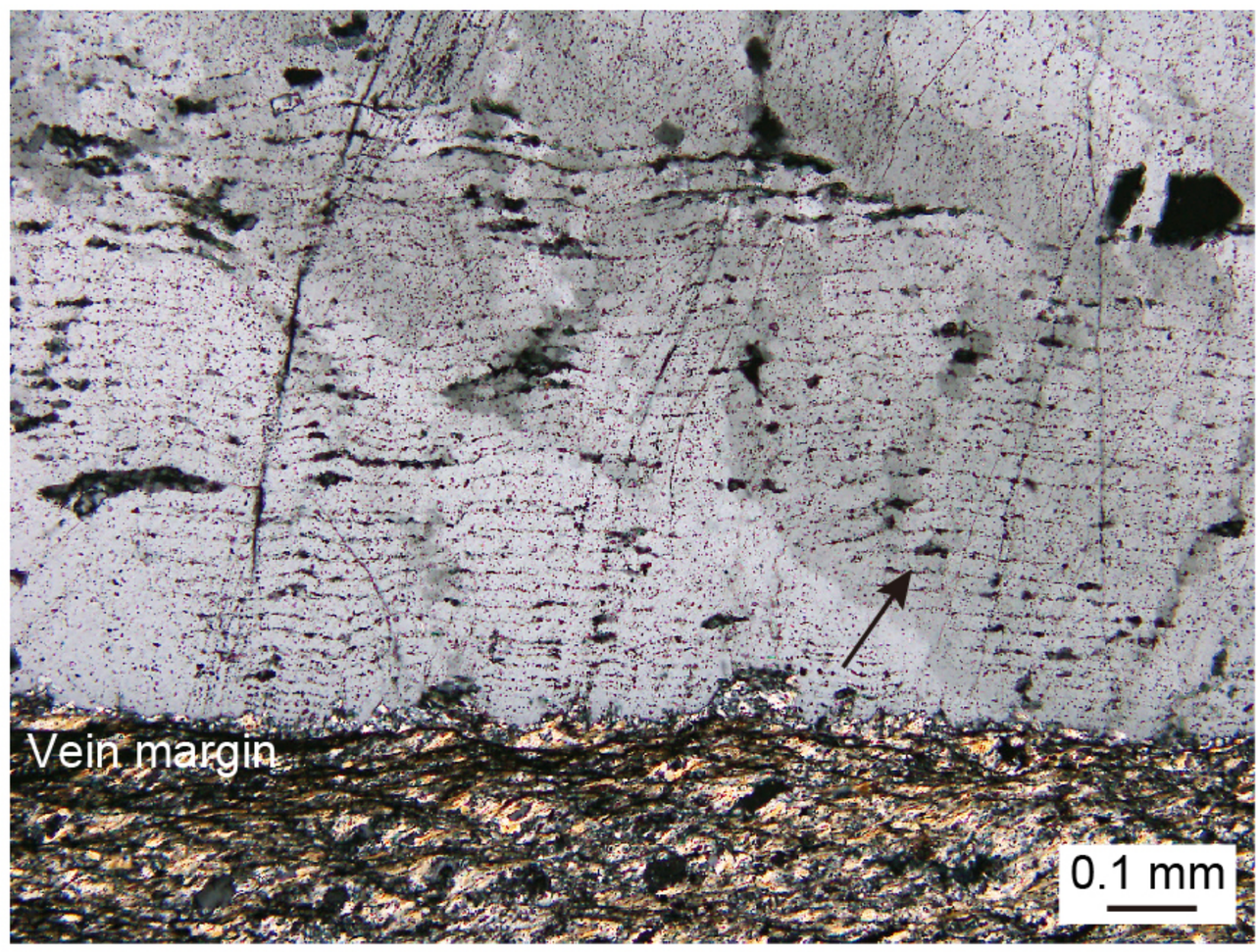
Vein margin
0.1 mm

d

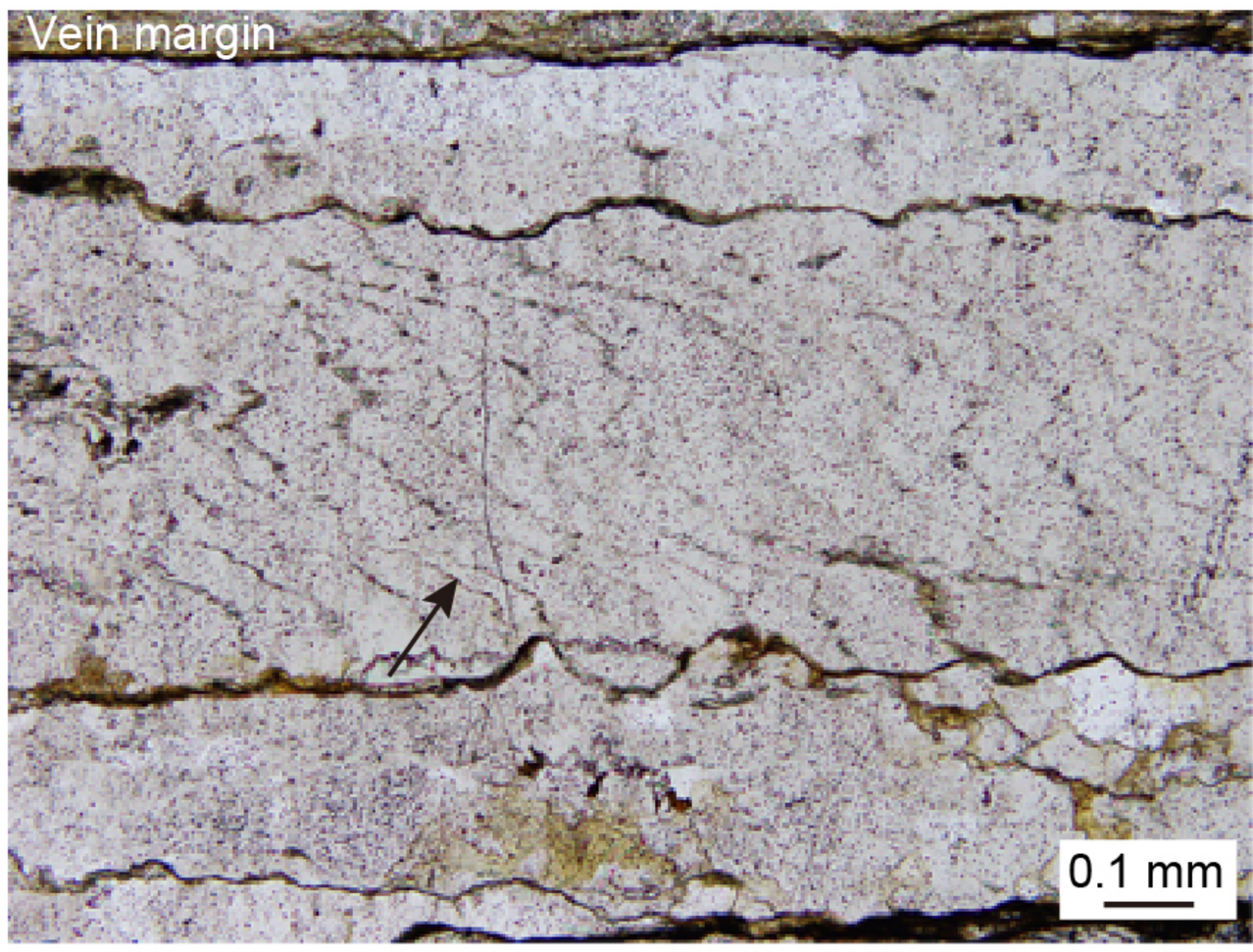
Vein margin
0.1 mm

e


Mélange foliation

f

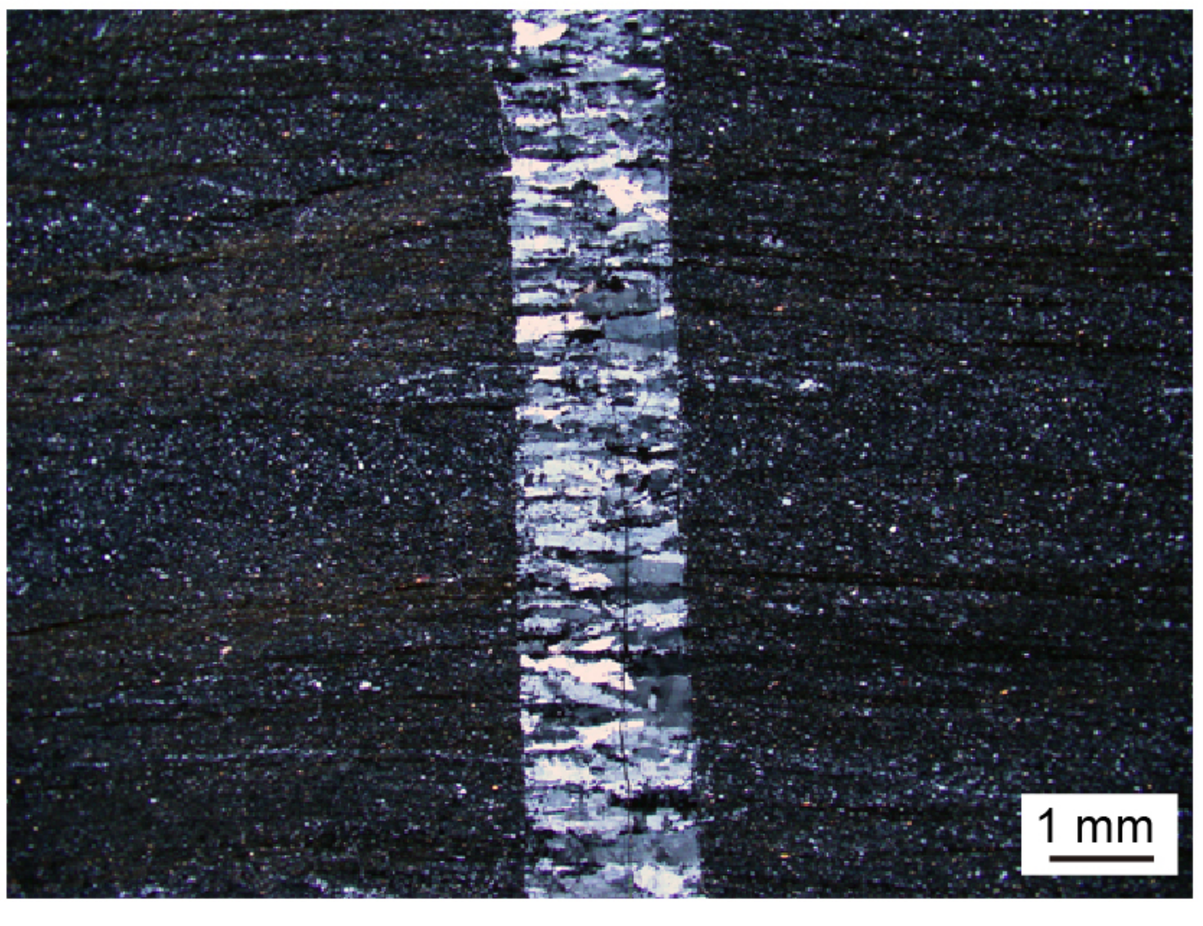
1 mm

g

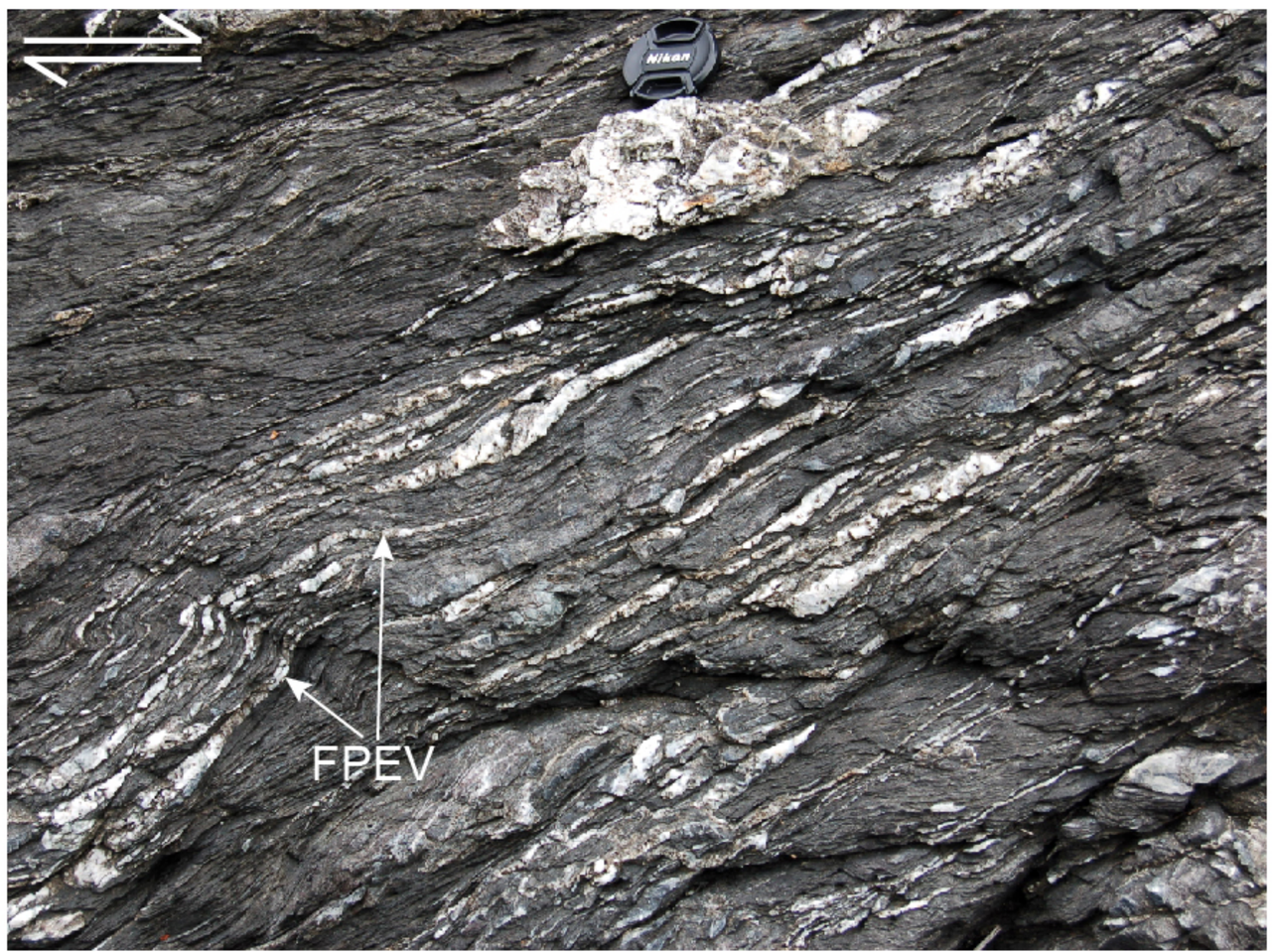
FPEV

h

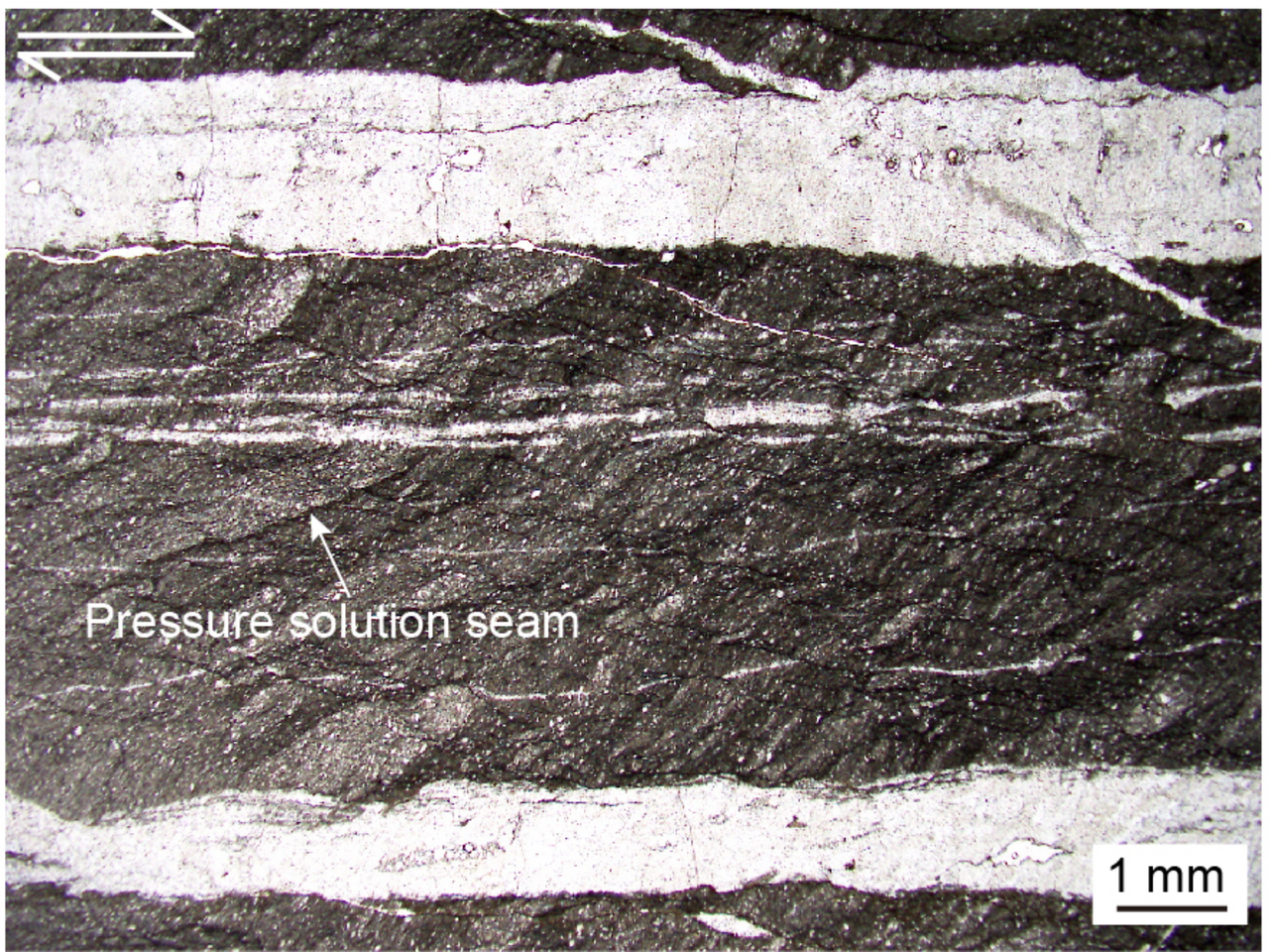
Pressure solution seam
1 mm

Figure 3.

a

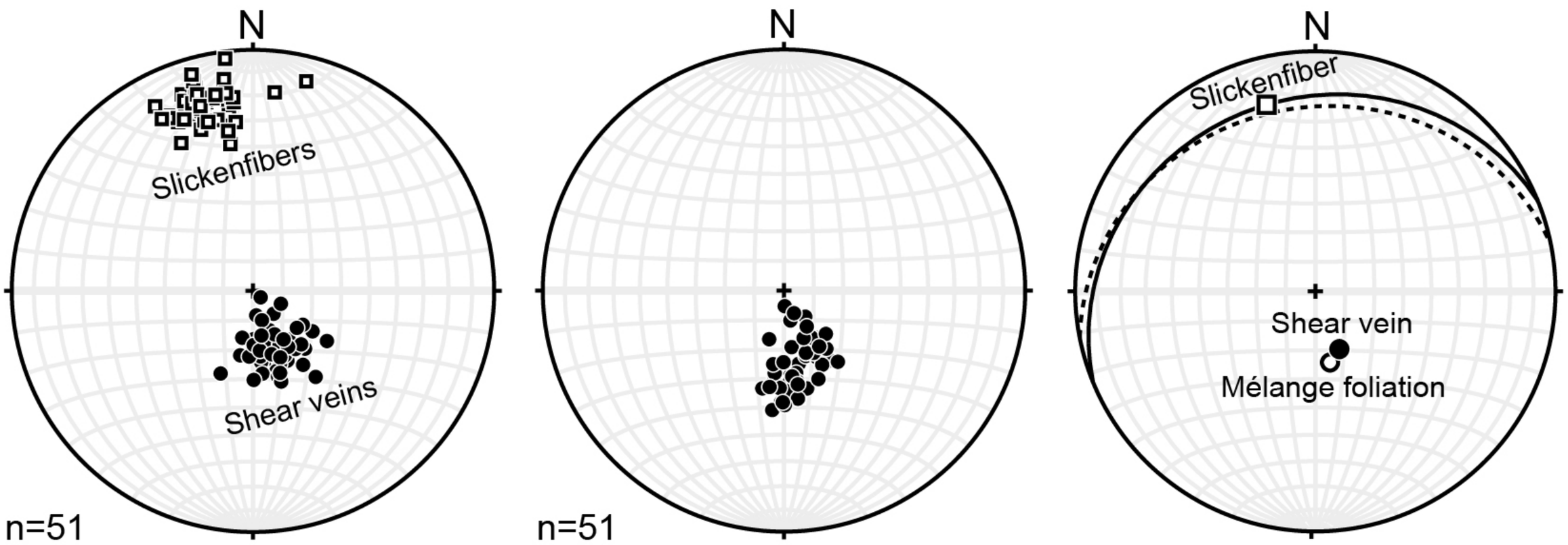
Shear veins
Mélange foliation
Average orientations
N
Slickenfibers
Shear veins
n=51
n=51
Slickenfiber
Shear vein
Mélange foliation

b

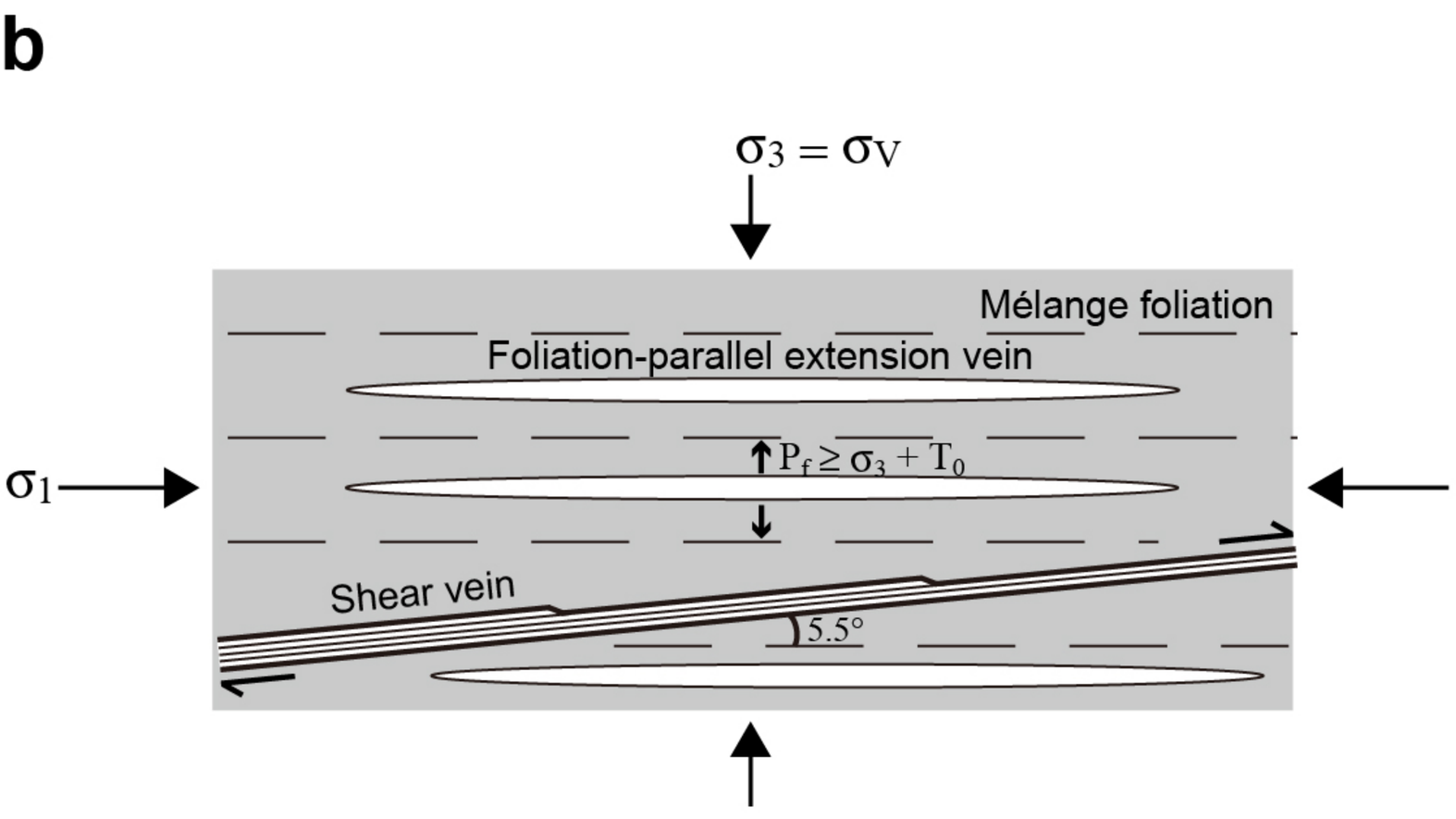
$\sigma_3 = \sigma_V$
Mélange foliation
Foliation-parallel extension vein
$P_f \geq \sigma_3 + T_0$
σ_1
Shear vein
5.5°

c

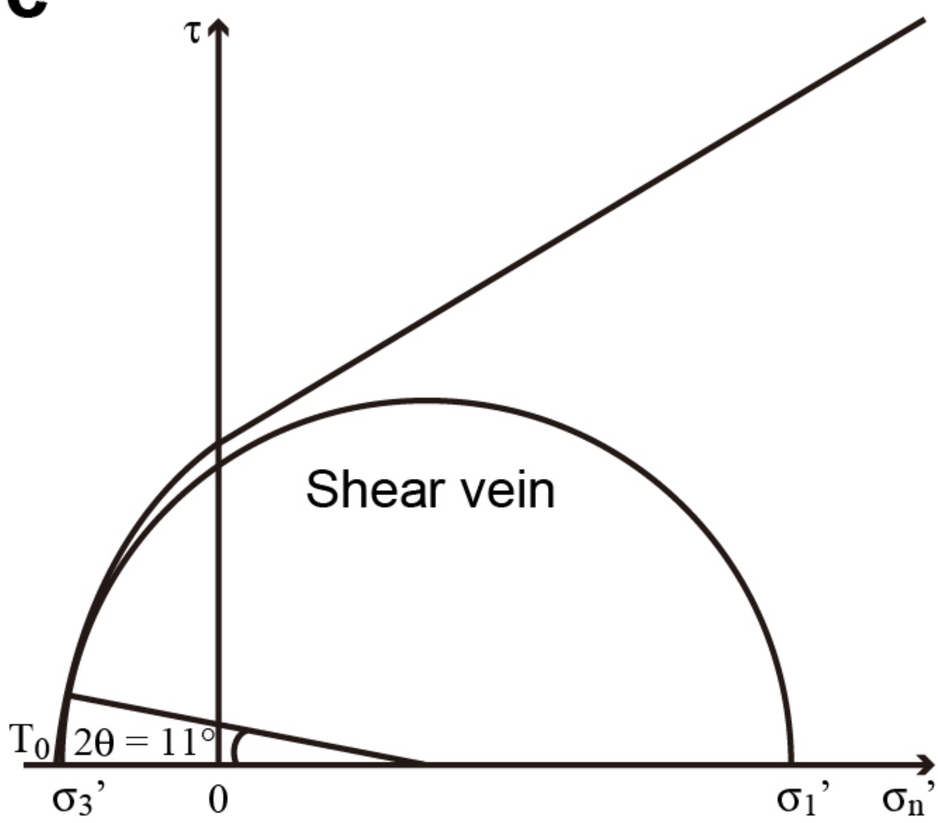
τ
Shear vein
T_0
2θ = 11°
σ_3'
0
σ_1'
σ_n'

d

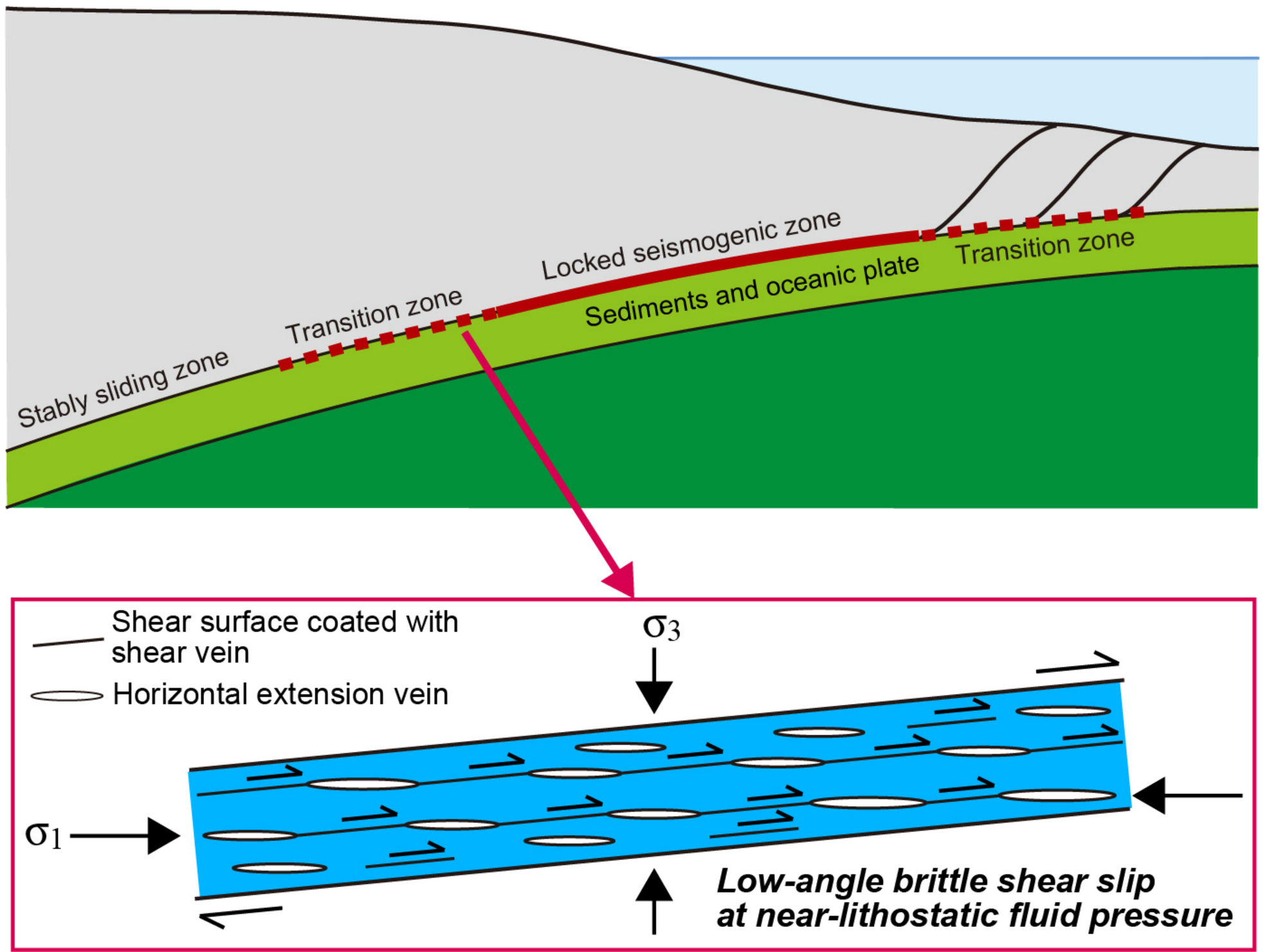
Stably sliding zone
Transition zone
Locked seismogenic zone
Sediments and oceanic plate
Transition zone
Shear surface coated with shear vein
Horizontal extension vein
σ_3
σ_1
Low-angle brittle shear slip
at near-lithostatic fluid pressure

Figure 4.

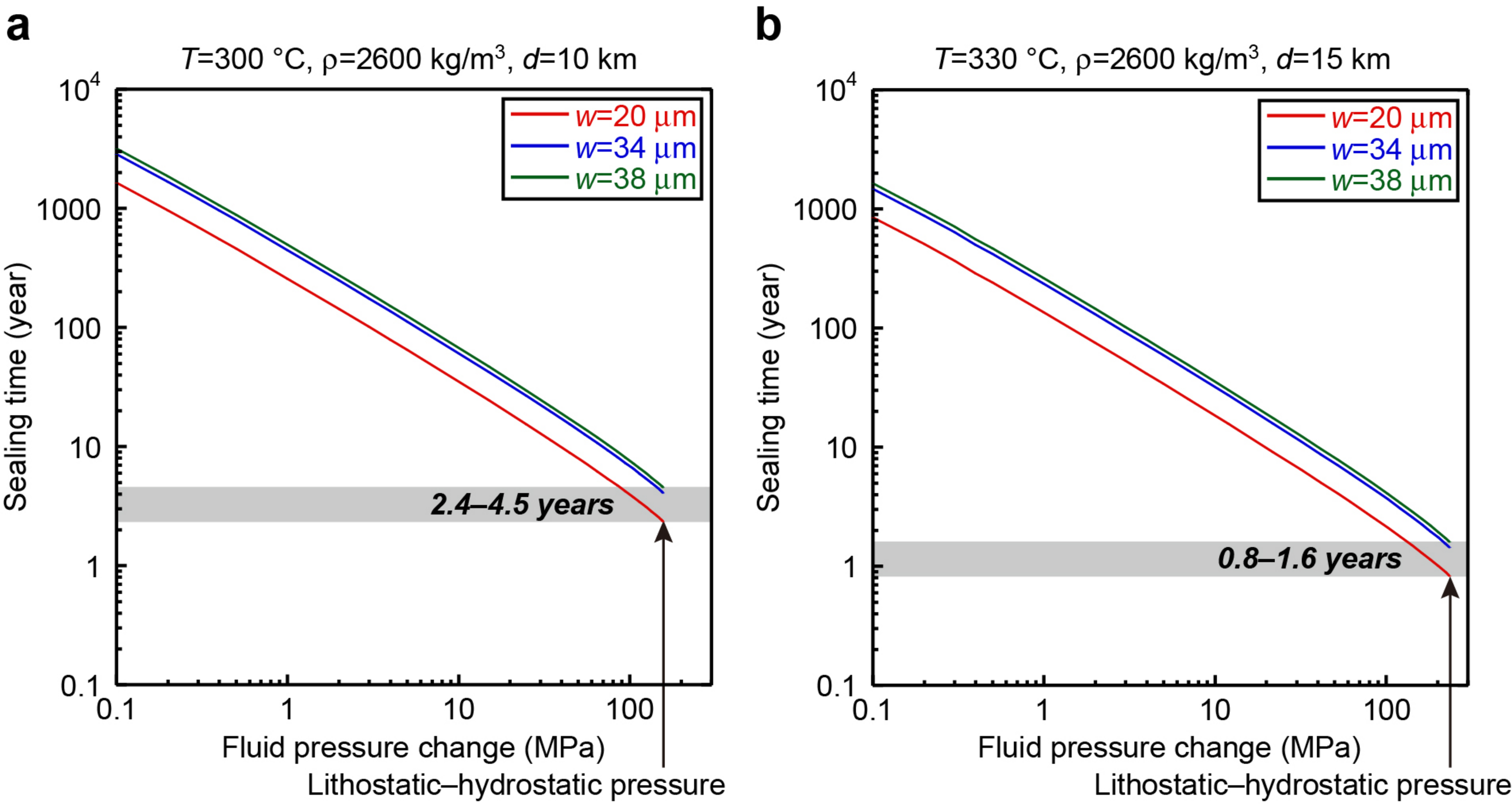
a
T=300 °C, ρ=2600 kg/m3, d=10 km
w=20 μm
w=34 μm
w=38 μm
2.4–4.5 years
Sealing time (year)
Fluid pressure change (MPa)
Lithostatic–hydrostatic pressure
b
T=330 °C, ρ=2600 kg/m3, d=15 km
w=20 μm
w=34 μm
w=38 μm
0.8–1.6 years
Sealing time (year)
Fluid pressure change (MPa)
Lithostatic–hydrostatic pressure